Propagation limits of flames in binary-fuel mixtures

Jan Palecka, Sam Goroshin, Jeffrey M. Bergthorson, Andrew J. Higgins
McGill University
Montreal, Québec, Canada

1 Introduction

Flames in homogeneous and heterogeneous systems are a result of complex interactions of multiple reaction steps. A qualitative analysis of these systems often starts with simple models of two consecutive or parallel reactions [1,2]. Due to the Arrhenius nature of reactions, such analysis usually employs sophisticated asymptotic methods and is not transparent due to a large number of dimensionless parameters. In our previous analysis of flame propagation in binary particulate suspensions of two chemically different solid fuels, we have proposed to approximate reaction rates by simple step functions [3] and, as a first approximation, the onset of each reaction can be assumed to occur when the suspension reaches the ignition temperature of a single particle. The approximation of the reaction rate by a step function allows exact analytical solutions of the linear differential equation that describes heat transfer across the flame, permitting the flame structure and the flame speed to be determined analytically. The present paper extends the analysis of flames with two parallel step-wise reactions to include heat losses. The analysis of the flame structure, propagation, and quenching with two parallel reactions is used to qualitatively interpret the complex behavior observed in our recent experiments studying flame propagation and quenching in aluminum-methane hybrid mixtures in narrow channels [4].

2 Model

Flame propagation and quenching in particulate suspensions was previously modelled by approximating the heat release profile by a single step-wise reaction [3]. One can consider a given mixture, with properties identified by the subscript 1, of a gas with a solid reactive suspension, seeded with varying concentrations of a second fraction, identified by 2. The fractions are chosen so that their ignition temperatures obey $\theta_{ig,1} < \theta_{ig,2}$. This also means the flame can reach either of two possible adiabatic temperatures $\theta_{ad,1} < \theta_{ad,2}$, where $\theta_{ad,1}$ and $\theta_{ad,2}$ are the adiabatic flame temperatures when one or both of the reactants release their heat. The governing equations for the one-dimensional propagation of two step-wise reactions R_1 and R_2, of each fraction respectively, can then be reduced to a single heat transfer equation:

$$\frac{1}{\kappa^2}\frac{d^2\theta}{d\xi^2} + \gamma\frac{d\theta}{d\xi} + \psi - \eta(\theta - 1) = 0 \qquad (1)$$

Correspondence to: jan.palecka@mail.mcgill.ca

For simplicity, the results are presented in a non-dimensional form, described in detail in [5] with the temperature θ, the spatial coordinate ξ, the propagation velocity κ, the concentration of the second fraction ϕ, the heat loss term η, and the heat capacity $\gamma=1+\upsilon\phi$, where υ is a constant. The respective values of the reaction term ψ over the flame, expressed in terms of the respective heats of reaction σ_i, are shown at the bottom of Fig.1. As shown on Fig.1, one can consider three different flame configurations. The first one corresponds to a flame where fraction 2 does not ignite, and, in fact, plays the role of an inert additive, with only one front due to the reaction R_1 (Fig. 1a). In the two remaining cases, the second reaction starts at $\xi=\chi$, the fronts are either detached with $\chi>1$ (Fig. 1b) or overlapped with $\chi<1$ (Fig. 1c). The generic solution of equation (1) can be written as:

$$\theta(\xi) = b_i e^{-\omega_1 \xi} + b_j e^{-\omega_2 \xi} - \frac{\psi}{\gamma} + 1 \quad \text{where} \quad \omega_{1,2} = \frac{1}{2}\left[\kappa^2\gamma \mp \sqrt{\kappa^4\gamma^2 + 4\kappa^2\eta}\right] \qquad (2)$$

As shown in Fig.1, the discontinuous nature of the reaction term ψ gives rise to either 3 or 5 distinct zones along ξ. In each zone, the temperature profile is described by (2) with a total of 6 or 10 unknown coefficients (b_i and b_j in each zone). These are found by equations obtained from matching the values of θ and the gradient, $d\theta/d\xi$, at the borders between zones, from the boundary conditions at -∞ and +∞, and imposing the temperature at $\xi=0$ and $\xi=\chi$ to be equal to the "ignition temperature" of each reaction. The remaining 1 or 2 equations are used to solve for the propagation velocity κ, and, in the case of two fronts, the position of the second front, χ. Thus, the problem is reduced from a differential equation to a system of algebraic ones. Some can be solved analytically while the roots of the rest are found with standard numerical methods.

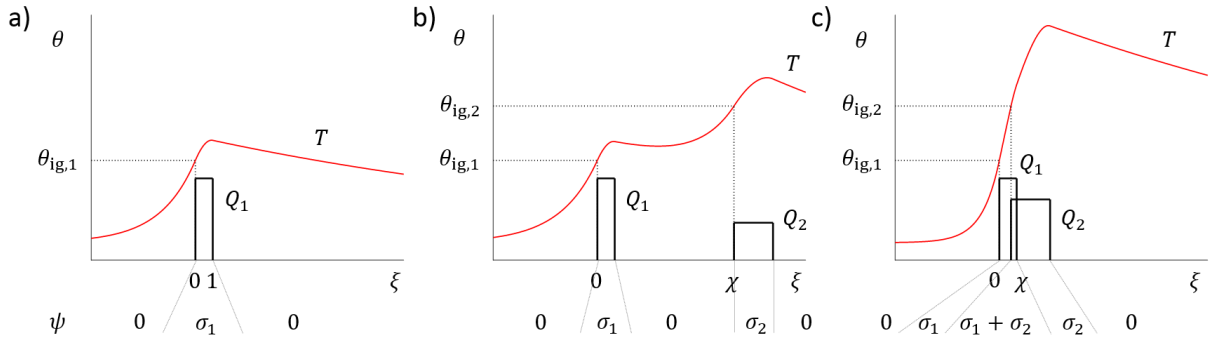

Figure 1. Temperature and heat release profiles across the flame for three flame configurations - single front (a.), two detached fronts (b.), two overlapping fronts (c.), along with intervals produced by changes in the values of the reaction term ψ.

3 Results

Figure 2a illustrates the evolution of the flame speed in the adiabatic system with increasing concentration of the second fraction. Three distinctive regimes of flame propagation can be noted. At low concentration, the second fraction cannot ignite as the adiabatic flame temperature, even when both the primary and secondary fuel release their chemical energy, is below the secondary ignition temperature. Thus, the second fraction plays the role of an inert additive and the flame speed declines. At a critical concentration of the second fraction, the adiabatic flame temperature reaches the secondary ignition temperature $\theta_{ig,2}$. A second front can form, but the flame speed of the resulting two-front flame is lower than the one of the one-front

case, and, consequently, the second front cannot couple to the first front which propagates at a higher speed. This corresponds to the separation regime first described in [1]. The flame speed of the second front increases with ϕ until both configurations propagate at the same speed, so that a second front can stabilize in the wake of the first one in a structure shown in Fig. 1b. At first, the distance between the first and second fronts tends to infinity but it rapidly shrinks with a further increase of the second fuel concentration. The detached fronts are thermally coupled, with the second one transferring heat and influencing the propagation of the first front. This is analogous to the control flame regime [1] for reactions with Arrhenius kinetics. Above some concentration ϕ, the fronts merge and propagate in an overlapped configuration in the merging regime, described in [1].

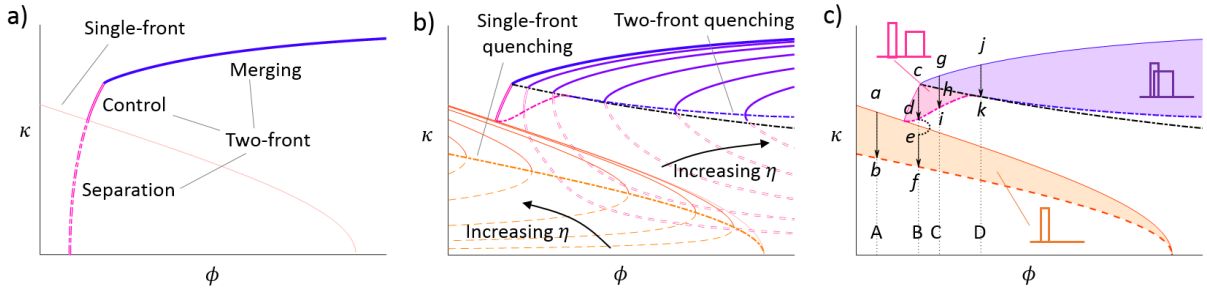

Figure 2. a) Dependence of the flame speed on dimensionless concentration of the inert fraction ϕ in a binary mixture showing the appearance of the 3 regimes of propagation in the adiabatic flame. b) Quenching behavior of both a single-front and two-front flames with increasing heat losses η. c) Quenching paths of different flame configurations.

The presence of heat losses from the system has a strong effect on the possible flame configurations. First, for a given ϕ, each configuration can adopt two flame speeds, one stable and physical and one unstable and usually unphysical, leading to two branches to each flame speed curve. In the case of an inert second fraction (flame structure in Fig. 1a), adding ϕ increases the total heat capacity γ and decreases the flame temperature. The flame speed of the physical solution decrease while the unphysical solution increases. As shown in Fig. 2b, the inclusion of heat loss initially shrinks, and then completely eliminates, the range of low concentrations of the inert fraction which can be added to this primary flame before it quenches. As for the two-front flame, the physical branch shows the flame speed increasing with increasing concentration of the second reactive fuel, and increasing total heat release, while the unphysical branch shows the flame speed decreasing with increasing heat release. Adding heat losses shrinks the range of concentrations where detached combustion fronts can be observed.

The flame quenching conditions are defined by the flame speed bifurcation points where stable and unstable solutions of the flame propagation equations merge. Figure 2b shows the quenching curve for the case of a single-front flame, seeded with an inert second fraction, that is subjected to heat losses, as well as the quenching curves for the second front. For intermediate concentrations, the second front quenches while detached from the first front. At higher concentrations of the second fuel, quenching of the second front occurs in the merged-flame regime and there is no solution for the single-front flame at these high levels of loading.

As Fig. 2c shows, the areas between the lines connecting values of the flame speeds at adiabatic conditions and the quenching curves define regions of the system parameters where steady-state propagation of the flame in a particular flame configuration is possible. These regions, corresponding to one-front, two-detached-front, and two-overlapped-front flames, are represented as shaded areas in Fig. 2c. The downward-pointing vertical arrows $a \rightarrow b$, $c \rightarrow f$, $g \rightarrow i$, and $j \rightarrow k$ in Fig. 2c indicate how the configuration of each flame

changes with an increase of the heat loss parameter η for different fixed values of the parameter ϕ, when all other system parameters are kept constant.

The single-front flame with the second fraction as an inert additive, which forms at low concentrations of the second fraction (Case A, path $a \rightarrow b$), responds to an increase of heat loss as a single-fuel flame. Its maximum temperature and flame speed progressively decrease from their adiabatic values until the flame quenches (point *b*).

For a flame with weakly coupled separated fronts (Case B, point *c*), addition of heat losses reduces the maximum flame temperature, and flame speed, and increases the separation distance between fronts until the secondary front quenches (point *d*). For the same level of heat loss, and the same set of other system parameters, a solution exists for a single-front flame with the second fraction acting as an inert additive (point *e*). The second front will thus quench, and the solution rapidly transitions from point *d* to point *e*. At point *e*, the front continues to propagate as a single flame front, albeit at much lower flame speed because the second fraction is now inert. Increasing the heat loss parameter further causes the single-front flame to completely quench at point *f*.

In Case C, the concentration of the second fuel fraction is high enough to form a flame with overlapped reaction fronts under adiabatic conditions (point *g*). Increasing heat losses η leads to a gradual increase in χ until it becomes larger than unity at point *h*, i.e. the fronts detach. A further increase in η leads to the quenching of the detached-front flame (point *i*) as described in Case B. At this concentration of ϕ, and the critical value of η, no single-front flame exists, and the entire flame quenches in unison.

Finally, for very high concentrations of the second fraction, where the flame fronts strongly overlap (Case D, point *j*), complete quenching of both reaction fronts occurs at point *k* before the fronts have a chance to detach, i.e. when χ is still below unity.

4 Comparison with experiments

The modeling results are used to interpret experimental tests obtained in a recent study by the present authors on flames in mixtures of methane and air, seeded with aluminum micron-sized particles, performed in tubes [4]. Flames either propagated or quenched in a set of narrow channels of adjustable width formed by equidistant parallel plates. The results of this previous experimental study are presented in Fig. 3a. This map summarizes the binary (or tertiary) flame propagation or quenching events, as well as the behavior of the flame in the main tube where heat losses are very minimal. It was found that, below a critical value of the aluminum concentration of about 300 g/m^3, the aluminum is acting primarily as an inert additive that reduces the primary flame temperature, its flame propagation speed, and that makes it easier for such dim orange flames to be quenched than for the pure methane-oxidizer flame without aluminum addition. At a critical value of the aluminum concentration, the flame appearance changes dramatically. It becomes almost white and very bright, indicating a large increase in the flame temperature that results from intense aluminum combustion in a secondary dust-flame front coupled to the primary methane flame, as was previously observed in flames stabilized on a burner [6]. At moderate aluminum loadings, the aluminum front quenches, and the brightness of the initially coupled aluminum-methane flame rapidly decreases, upon reaching the channels. A set of dim orange methane-air flamelets, similar to flames at lower aluminum concentrations, propagate through the channels. As these methane flamelets re-enter the larger tube, they coalesce back into a bright white flame, indicating the re-establishment of coupled methane and aluminum flame fronts. The maximum channel width at which the aluminum front quenches decreases with increasing aluminum concentration, as shown in Fig. 3a. At very high concentrations of aluminum, the entire bright

coupled aluminum-methane flame is either able to propagate through the channels, or it quenches as a whole as soon as it enters the quenching-plate assembly.

In order to compare the model to the experimental results, Fig. 2 was recast into a graph analogous to the experimental map. Using the fact that η is proportional to d^{-2} [5], d being the channel width, leads to the graph in Fig. 3b. The detached top strips in Fig. 3 corresponds to the flame configuration in the wide tube for the experimental graph and to a channel of infinite width, or the adiabatic flame solution, for the theoretically predicted flame map. All regions in the κ–ϕ plane along with the flame configurations in Fig.2 are also present in Fig. 3b, together with the pathways $a \rightarrow b$, $c \rightarrow f$, $g \rightarrow i$, and $j \rightarrow k$ (Cases A to D) discussed previously. It is easy to see that all these theoretically predicted cases have an experimental analog. At aluminum concentrations below 300 g/m^3, the aluminum flame front does not form and the flame quenches as a single front flame (path $a \rightarrow b$, Case A). The sudden increase of the flame brightness in the wide tube above aluminum concentrations of 300 g/m^3 indicates the appearance of an aluminum combustion front that is initially detached. The detached-fronts flame is very susceptible to heat losses and, thus, cannot exist in a narrow channel. The aluminum combustion front quenches upon entering the quenching plate assembly but the flame continues to propagate as a methane flame seeded with relatively inert aluminum powder (with a state between e and f depending on the channel width). As it exits the channels into the tube with negligible heat losses, the flame reverts back to a coupled methane-aluminum front structure (reverse path $e \rightarrow f \rightarrow c$). It quenches inside the channel at some critical width ($c \rightarrow f$).

At high aluminum concentrations, corresponding to Case D, both fronts merge. Due to the very high specific heat capacity of the mixture, the methane flame in this case cannot propagate without support from the aluminum combustion. Therefore, the merged fronts either propagate through the channels together or, in sufficiently narrow channels, they quench in unison (point k). For single-front flames, the model also correctly predicts the experimentally-observed increase of the flame quenching channel width with an increase in the aluminum concentration. The model, however, predicts a reversed trend and a sharp decrease in the quenching diameter for a coupled methane-aluminum front structure at high aluminum concentrations. The model formulation accounts neither for the competition of methane and aluminum for oxygen in physically coupled fronts nor for the dependence of the reaction rate on the concentration of oxygen in the fuel-rich flames. Both effects will considerably decrease the flame temperature, the reaction rate, and,

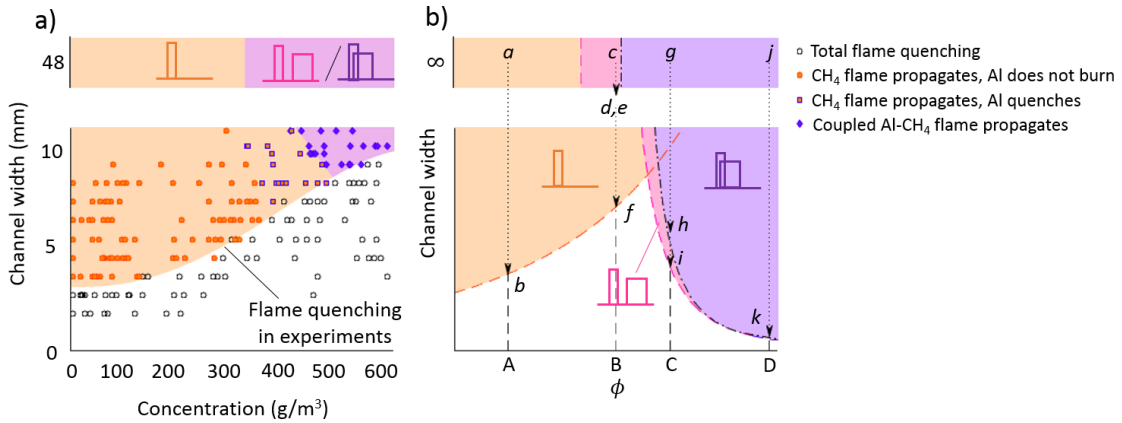

Figure 3. Maps of the flame propagation/quenching events in channels of different width and at different concentrations of aluminum in the fuel mixture. a) Obtained from experiment and b) predicted by the model.

consequently, the speed of the flame, resulting in higher quenching distances. This indicates a limit of applicability of the model.

4 Conclusion

Flame propagation in a binary mixture of two independently reacting fuels was investigated analytically by assuming externally-imposed ignition temperatures to initiate the two reaction fronts, step-wise reaction rates, and volumetric heat losses. In spite of the model simplicity, it is able to reproduce the different flame propagation regimes, corresponding to detached and merged reaction fronts, previously identified in the literature. It was found that, for the detached-front structure that occurs at intermediate values of the second fuel concentration, an increase in heat losses can cause only the second front to quench while the first flame front will continue to propagate, albeit with sharply reduced speed. In contrast, for the flame with merged combustion zones at high loadings of the second fuel, the separate quenching of individual reacting fuels is impossible and the flame can only propagate, or be quenched, in unison. The predicted flame behavior was found to be in qualitative agreement with our recent experimental results on flame propagation and quenching in aluminum-methane-oxidizer mixtures, and the model enables these results to be understood and explained because of its simplicity.

References

[1] Khaikin B., Filonenko A., Khudyaev S. (1968). Flame propagation in the presence of two successive gas-phase reactions. Combust. Explos. Shock Waves 4: 343.

[2] Berman VS., Ryazantsev YS. (1975). Asymptotic analysis of stationary propagation of the front of a parallel exothermic reaction. J. Appl. Math. Mech. 39:286.

[3] Goroshin S., Kolbe M., Lee JHS. (2000). Flame speed in a binary suspension of solid fuel particles. Proc. Combust. Inst. 28: 2811.

[4] Palecka J., Julien P., Goroshin S., Bergthorson JM., Frost DL., Higgins AJ. (2015). Quenching distance of flames in methane-aluminum hybrid mixtures. Proc. Combust. Inst. 35: 2463.

[5] Goroshin S., Bidabadi M., Lee JHS. (1996). Quenching distance of laminar flame in aluminum dust clouds. Combust. Flame 105: 147.

[6] Julien P., Soo M., Goroshin S., Frost DL.,Bergthorson JM., Glumac N., Zhang F. (2014). Combustion of Aluminum Suspensions in Hydrocarbon Flame Products. J. Propuls. Power 30: 1047.